JCI insight

RESEARCH ARTICLE

Activation of CAR and non-CAR T cells within the tumor microenvironment following CAR T cell therapy

Pei-Hsuan Chen,[1] Mikel Lipschitz,[1] Jason L. Weirather,[1] Caron Jacobson,[2] Philippe Armand,[2] Kyle Wright,[3] F. Stephen Hodi,[1,2] Zachary J. Roberts,[4] Stuart A. Sievers,[4] John Rossi,[4] Adrian Bot,[4] William Go,[4] and Scott J. Rodig[1,3]

[1]Center for Immuno-Oncology and [2]Department of Medical Oncology, Dana-Farber Cancer Institute, Boston, Massachusetts, USA. [3]Department of Pathology, Brigham and Women's Hospital, Boston, Massachusetts, USA. [4]Kite, a Gilead company, Santa Monica, California, USA.

Mechanisms of chimeric antigen receptor (CAR) T cell–mediated antitumor immunity and toxicity remain poorly characterized because few studies examine the intact tumor microenvironment (TME) following CAR T cell infusion. Axicabtagene ciloleucel is an autologous anti-CD19 CAR T cell therapy approved for patients with large B cell lymphoma. We devised multiplex immunostaining and ISH assays to interrogate CAR T cells and other immune cell infiltrates in biopsies of diffuse large B cell lymphoma following axicabtagene ciloleucel infusion. We found that a majority of intratumoral CAR T cells expressed markers of T cell activation but, unexpectedly, constituted ≤5% of all T cells within the TME 5 days or more after therapy. Large numbers of T cells without CAR were also activated within the TME after axicabtagene ciloleucel infusion; these cells were positive for Ki-67, IFN-γ, granzyme B (GzmB), and/or PD-1 and were found at the highest levels in biopsies with CAR T cells. Additionally, non-CAR immune cells were the exclusive source of IL-6, a cytokine associated with cytokine release syndrome, and were found at their highest numbers in biopsies with CAR T cells. These data suggest that intratumoral CAR T cells are associated with non-CAR immune cell activation within the TME with both beneficial and pathological effects.

Introduction

Chimeric antigen receptors (CARs) are synthetic immunoreceptors expressed by T cells that specifically target cancer cells (1–3). Autologous CARs use the patients' T cells, which are engineered and expanded ex vivo and infused back into patients with lymphodepleting chemotherapy to enhance further expansion in vivo. CAR T cells recognizing the B cell–specific antigen CD19 are effective in the treatment of a variety of B cell malignancies (1, 4–9). Axicabtagene ciloleucel is a commercially approved, engineered autologous anti-CD19 CAR T cell therapy in which the extracellular domain of the CAR has a single-chain variable fragment targeting CD19 and the intracellular domain has the signaling motifs of CD3ζ and CD28 to promote T cell activation (10).

The ZUMA-1 study was a single-arm, phase I–II, multicenter trial of axicabtagene ciloleucel for patients with refractory large B cell lymphoma (11, 12). Among 101 treated patients, the objective response rate was 82%, the complete response rate was 54%, and the overall survival was 52%, with a median of 15.4 months of follow-up (11). The 2-year follow-up data suggested that these responses are durable (11). However, most patients experienced 1 or more grade 3 or higher adverse events (AEs), including neutropenia (78%), anemia (43%), neurologic events (28%), and cytokine release syndrome (CRS, 13%) (11). Based upon the trial results, axicabtagene ciloleucel was approved by the Food and Drug Administration for the third-line treatment of diffuse large B cell lymphoma (DLBCL), primary mediastinal (thymic) large B cell lymphoma, high-grade B cell lymphoma, and transformed follicular lymphoma (13). As a result, axicabtagene ciloleucel is increasingly used in the commercial setting for the treatment of relapsed/refractory B cell malignancies, despite the potential for serious AEs (14).

Detailed mechanisms of CAR T cell tumoricidal activity and toxicity remain poorly understood, due, in part, to a lack of information on the events that occur in the tumor microenvironment (TME) after product infusion (15–18). In correlative biomarker studies performed as part of ZUMA-1, patients with higher

Authorship note: PHC and ML contributed equally to this work.

Conflict of interest: SJR receives research support from Kite, a Gilead company; Merck; Bristol-Myers Squibb; and Affimed Therapeutics. SJR is on a scientific advisory boards for Immunitas Inc. and RareCyte Inc. FSH reports grants, personal fees, and other fees from Bristol-Myers Squibb; personal fees from Merck and EMD Serono; grants, personal fees, and other fees from Novartis; personal fees from Takeda, Surface, Genentech/Roche, Compass Therapeutics, Apricity, Bayer, Aduro, Partners Therapeutics, Sanofi, Pfizer, Pionyr, 7 Hills Pharma, Verastem, Torque, Rheos, Kairos, Bicara, Psioxus Therapeutics, and Amgen; and other fees from Pieris Pharmaceutical, Boston Pharmaceuticals, and Zumutor. In addition, FSH has a patent for treating MICA-related disorders (20100111973) with royalties paid, a patent for tumor antigens and uses thereof (7250291), a pending patent for angiopoietin-2 biomarkers predictive of anti-immune checkpoint response (20170248603), a pending patent for compositions and methods for identification, assessment, prevention, and treatment of melanoma using PD-L1 Isoforms (20160340407), a pending patent for therapeutic peptides (20160046716), a pending patent for therapeutic peptides (20140004112), a pending patent for therapeutic peptides (20170022275), a pending patent for therapeutic peptides (20170008962), a pending patent for methods of using pembrolizumab and trebananib, a patent for vaccine compositions and methods for restoring NKG2D pathway function against cancers (10279021), and a patent for antibodies that bind to MHC class I polypeptide-related sequence A (2008036981A9). ZJR, SAS, JR, AB, WG are employees of Kite, a Gilead company.

Submitted: December 11, 2019
Accepted: May 20, 2020
Published: May 28, 2020.

Reference information: *JCI Insight*. 2020;5(12):e134612. https://doi.org/10.1172/jci.insight.134612.

numbers of CAR T cells measured in blood within 2 weeks of infusion had higher rates of objective and durable response (11, 19). Similarly, patients with higher levels of select serum cytokines, including IL-6, had higher rates of AEs, including CRS (11, 20). Nevertheless, it is unclear whether the characteristics of CAR T cells and immune cells lacking CAR (non-CAR) in peripheral blood reflect those at the site of malignancy. Unanswered questions include the extent of CAR T cell residency within the TME, the degree of activation among CAR T cells that engage tumor, the extent and relevance of non-CAR immune cells within the TME, the effects of CAR T cells on non-CAR immune cells, and whether events within the TME are directly or indirectly responsible for toxicity. Here, we use what we believe to be novel multiplex immunostaining and ISH assays to identify, quantify, and characterize both CAR T cells and non-CAR cells within the TME of patients with DLBCL enrolled in the ZUMA-1 trial.

Results

We optimized and applied multiplex immunofluorescence (mIF) staining, imaging, and image analysis to separate cohorts of FFPE biopsy samples from patients with (a) de novo DLBCL subsequently treated with standard therapies (n = 15), (b) relapsed/refractory DLBCL before axicabtagene ciloleucel treatment (n = 7), and (c) radiographically evident tumor 5–30 days (median 10 days) after axicabtagene ciloleucel treatment (n = 17). The latter set of biopsies was further divided into those from patients with an objective response to therapy (with best overall response [BOR] of complete response or partial response, n = 14) and those from patients without an objective response (BOR of stable disease or progressive disease, n = 3, Supplemental Table 1; supplemental material available online with this article; https://doi.org/10.1172/jci.insight.134612DS1).

An optimized mIF panel using antibodies to simultaneously identify DLBCL cells (anti-Pax5), T cells (anti-CD3, anti-CD4, anti-CD8), and postactivation/"exhausted" T cells (anti–PD-1) highlighted malignant B cells and variable numbers of nonmalignant T cells in the expected histopathological patterns when applied to the FFPE biopsy samples (Figure 1). By quantitative analysis, we found that the median density of Pax-5–positive malignant B cells within posttreatment biopsies from patients with an objective response to axicabtagene ciloleucel was significantly lower compared with that within diagnostic biopsies (median 3.5 vs. 6042 cells/mm^2, $P < 0.001$), pretreatment biopsies (vs. 8790 cells/mm^2, $P < 0.001$), or posttreatment biopsies from patients without an objective response to axicabtagene ciloleucel (vs. 5489 cells/mm^2, $P = 0.02$) for the time points sampled (5–30 days after axicabtagene ciloleucel, Figure 1A). We also found that the median density of CD3-positive T cells in posttreatment biopsies from patients with an objective response to axicabtagene ciloleucel was higher compared with that in diagnostic biopsies (median 1658 vs. 959 cells/mm^2), pretreatment biopsies (vs. 426 cells/mm^2), or posttreatment biopsies from patients without an objective response (vs. 311 cells/mm^2), but these differences were not statistically significant (Figure 1B). The trend toward increased T cells in posttreatment biopsies from patients with an objective response was primarily driven by a relative increase in CD8-positive T cells and decrease in CD4-positive T cells in the TME (Supplemental Figure 1). Upon more detailed evaluation, we found that the percentage of T cells coexpressing CD8 and PD-1 was significantly higher in posttreatment biopsies from patients responsive to axicabtagene ciloleucel compared with that in diagnostic (median 26% vs. 2.5%, $P < 0.001$) and pretreatment (vs. 9.5%, $P = 0.04$) biopsies (Figure 1C). A similar increase was not found for CD4-positive PD-1–positive T cells (Figure 1D). These data suggest that changes in the intratumoral T cell population are more significant for the types of T cells than total T cell numbers 5 or more days after axicabtagene ciloleucel. More specifically, there is a relative increase in cytotoxic T cells with a postactivation/exhausted phenotype.

We next optimized an immunofluorescence-based protocol to identify CAR-expressing T cells in FFPE tissue sections using a rabbit monoclonal antibody recognizing a specific epitope within the CAR (clone KIP1). We detected robust CAR expression on FFPE cells transduced with retrovirus containing the *CAR* transgene, but no CAR expression on FFPE cells untransduced with retrovirus or on cells in diagnostic or pretreatment biopsies (Figure 2A). We observed CAR T cells in 6 of 18 biopsies (33%) after product infusion, and all biopsies with CAR T cells were obtained soon after therapy (7–9 days) (Figure 2, A and B). Unexpectedly, CAR T cells made up only 1%–5% of total T cells within the TME (Figure 2B). To confirm these results, we optimized immunostaining with a second rabbit monoclonal antibody recognizing a distinct CAR epitope (clone KIP3). mIF performed with this second antibody also revealed robust CAR expression on FFPE cells transduced with retrovirus containing the *CAR* transgene but not on FFPE cells untransduced with retrovirus or on cells in diagnostic or pretreatment biopsies (Figure 2C).

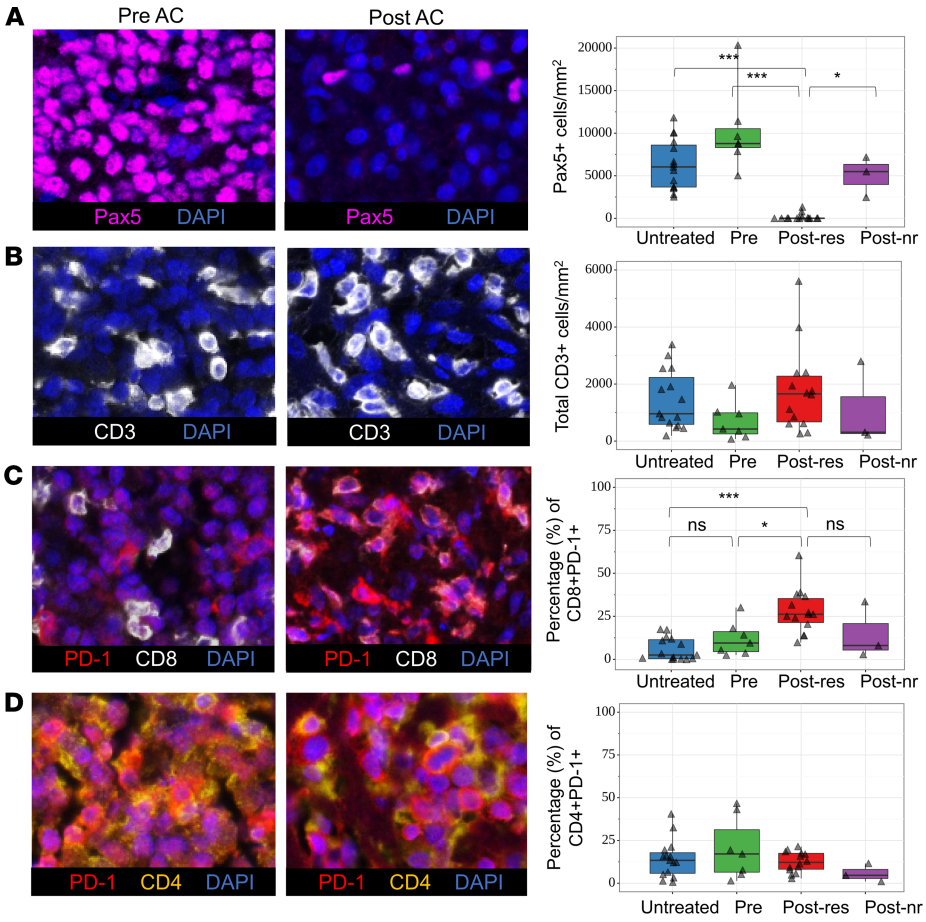

Figure 1. Resolution of lymphoma and T cell activation/exhaustion within the diffuse large B cell lymphoma microenvironment early after axicabtagene ciloleucel. Multiplex immunofluorescence (mIF) images of representative FFPE DLBCL biopsy samples before (left) and following (middle) axicabtagene ciloleucel (AC), and quantitative mIF data (right) from DLBCL biopsy samples obtained at diagnosis (Untreated, n = 15, blue), before axicabtagene ciloleucel (Pre, n = 7, green), and following axicabtagene ciloleucel divided according to a best overall response (Post-res [complete response or partial response], n = 14, red; Post-nr [stable disease or progressive disease], n = 3, purple). (**A**) Representative images of anti-Pax5 staining, highlighting malignant B cells (magenta), and DAPI highlighting cell nuclei (blue) and Pax5$^+$ malignant B cell densities within the indicated sample groups. The Kruskal-Wallis (KW) test indicated a significant difference in cell densities between conditions (P < 0.001). (**B**) Representative images of anti-CD3 staining, highlighting T cells (white), and DAPI highlighting cell nuclei (blue) and CD3$^+$ T cell densities within the indicated sample groups. The KW test was not significant (P = 0.2). (**C**) Representative images of anti-CD8 staining, highlighting cytotoxic T cells (white), anti–PD-1, highlighting exhausted cells (red), and DAPI (blue) and the percentage of CD8$^+$PD-1$^+$ cells among total T cells within the indicated sample groups. The KW test was significant (P < 0.001). (**D**) Representative images of anti-CD4 staining, highlighting T helper cells (yellow), anti–PD-1 (red), and DAPI (blue) and the percentage of CD4$^+$ PD-1$^+$ cells among total T cells within the indicated groups. The KW test was not significant (P = 0.3). Brackets above the box-and-whisker plots indicate comparators in 2-sided Mann-Whitney U tests followed by Benjamini-Hochberg (BH) correction for multiple tests. *adjusted P < 0.05, **adjusted P < 0.01, ***adjusted P < 0.001.

Immunostaining with the second anti-CAR antibody confirmed the prior findings, specifically that ≤5% of T cells within the TME after product infusion expressed detectable CAR protein (Figure 2D). Next, we optimized an ISH protocol using an antisense probe targeting the *CAR* transcript (Figure 2, E and F) to control for the possibility that the lack of CAR protein expression was due to CAR protein downregulation. We found cells expressing *CAR* transcript in 6 of 14 samples after axicabtagene ciloleucel, and, when observed, *CAR*-expressing cells comprised 4%–12% of all cells within the TME (Figure 2F). Overall, the median percentage of cells expressing *CAR* transcript was much lower than the percentage of cells expressing CD3 (median 6.6% vs. 43%, P = 0.005, Supplemental Figure 2). Together, the immunohistochemical and in situ data suggest that CAR T cells make up a small percentage of intratumoral T cells ≥5 days following axicabtagene ciloleucel infusion in DLBCL.

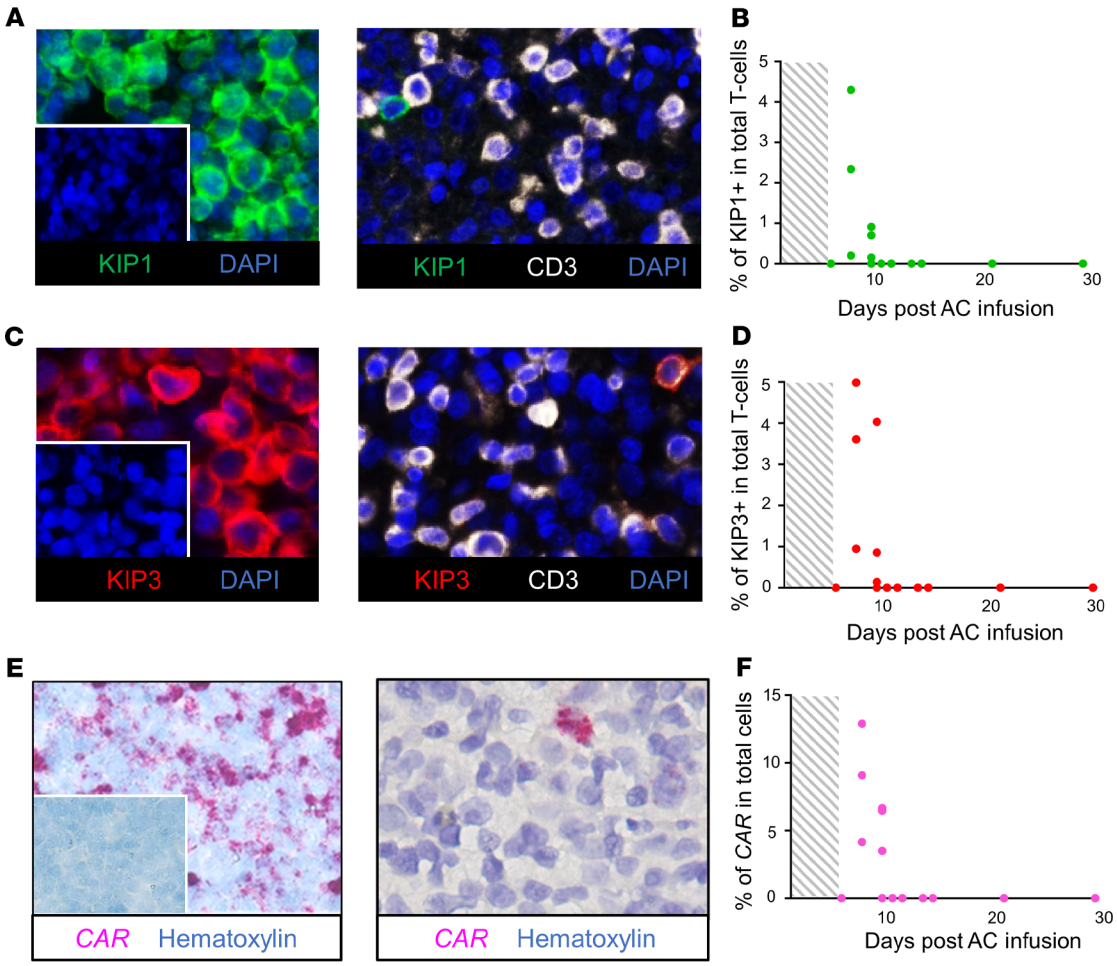

Figure 2. CAR and non-CAR T cells within the diffuse large B cell lymphoma microenvironment after axicabtagene ciloleucel. (**A**) Representative images of immunofluorescence (IF) staining with a monoclonal anti-CAR antibody (clone KIP1, green) and DAPI (for cell nuclei, blue) performed on FFPE cells previously transduced (left, main) or untransduced (left, inset) with retrovirus encoding the *CAR* transgene. Multiplex IF staining a biopsy sample obtained 7 days after axicabtagene ciloleucel infusion (right) with anti-CAR (KIP1 antibody, green), anti-CD3 (white), and DAPI (blue) showing CAR expression on a subset of T cells. (**B**) The number of days after axicabtagene ciloleucel infusion a biopsy was obtained and the percentage of T cells expressing the CAR antigen, as detected with the KIP1 antibody. (**C**) Representative images of IF staining with a monoclonal anti-CAR antibody (clone KIP3, red) and DAPI (blue) performed on FFPE cells previously transduced (left, main) or untransduced (left, inset) with retrovirus encoding the *CAR* transgene. Multiplex IF staining a biopsy sample obtained 7 days after axicabtagene ciloleucel infusion (right) with anti-CAR (KIP3 antibody, red), anti-CD3 (white), and DAPI (blue) and showing CAR expression on a subset of T cells. (**D**) The number of days after axicabtagene ciloleucel infusion a biopsy was obtained and the percentage of T cells expressing the CAR antigen, as detected with the KIP3 antibody. (**E**) Representative images of ISH with an antisense probe for the *CAR* transcript (red) and hematoxylin staining (for nuclei, blue) performed on FFPE cells previously transduced (left, main) or untransduced (left, inset) with retrovirus encoding the *CAR* transgene. ISH performed on a biopsy sample obtained 7 days after axicabtagene ciloleucel infusion (right) with anti-*CAR* (red) and with hematoxylin staining (blue) showing *CAR* transcripts in a subset of cells. (**F**) The number of days after axicabtagene ciloleucel infusion a biopsy was obtained and the percentage of cells expressing *CAR* transcript as detected by ISH. Original magnification, ×200 (**A**, **C**, and **E**, including insets).

Upon T cell receptor and coreceptor ligation, T cells enter cell cycle, express proinflammatory effector molecules, and, depending upon microenvironmental cues, initiate a differentiation program resulting in T cell exhaustion (21, 22). We interrogated the CAR T cell population for markers of ongoing or prior T cell activation across posttreatment biopsy specimens and found that, on average, 89% of CAR T cells expressed the cell cycle marker Ki-67 (Figure 3A), 76% expressed T cell postactivation/exhaustion marker PD-1 (Figure 3B), and 31% expressed the cytotoxic granule protein GzmB (Figure 3C). Ki-67 and PD-1 were often, but not always, seen on distinct CAR T cells. Through ISH studies, we found that, on average, 74% of *CAR*-transcript expressing cells expressed the transcripts encoding the proinflammatory cytokine IFN-γ (*IFNG*, Figure 3D) (23). Together, these data indicate that most CAR T cells have phenotypic evidence for ongoing or prior activation.

Next, we investigated the nature and activation status of non-CAR T cells in the TME. We identified small numbers non-CAR T cells and other immune cells positive for Ki-67, PD-1, and/or GzmB before

axicabtagene ciloleucel treatment (Figure 4, A–F). We observed significantly more Ki-67–positive non-CAR T cells within posttreatment biopsies that contained CAR T cells in comparison to pretreatment biopsies (median 1411 vs. 125 cells/mm^2, $P = 0.008$) and to posttreatment biopsies without CAR T cells (vs. 311 cells/mm^2, $P = 0.005$, Figure 4B). We also observed significantly more PD-1–positive non-CAR T cells within posttreatment biopsies that contained CAR T cells in comparison to pretreatment biopsies (median 824 vs. 224 cells/mm^2, $P = 0.02$) and to posttreatment biopsies lacking CAR T cells (vs. 389 cells/mm^2, $P = 0.02$, Figure 4C). We observed a trend toward more GzmB-positive non-CAR T cells ($P = 0.05$) and found significantly more GzmB-positive immune cells ($P = 0.03$) in posttreatment biopsies containing CAR T cells in comparison with posttreatment biopsies without CAR T cells (Figure 4, E and F). Overall, the numbers of non-CAR T cells and immune cells that expressed Ki-67, PD-1, and/or GzmB exceeded CAR T cells by 5- to 10-fold in biopsies where CAR T cells were detected (Supplemental Figure 3, A–C).

We next assessed whether cells histologically consistent with immune cells and lacking *CAR* transcripts (non-*CAR* cells) expressed *IFNG* in the posttreatment biopsies. We identified frequent non-*CAR* cells that expressed *IFNG* when *CAR*-positive cells were present in the biopsy (median 76 cells/mm^2 of non-*CAR* cells, Figure 4, G and H). In contrast, we rarely identified non-*CAR* cells that expressed *IFNG* when *CAR*-positive cells were absent from the biopsy (median 3.0 cells/mm^2 of non-*CAR* cells, $P = 0.002$, Figure 4H). The density of non-*CAR* cells that expressed *IFNG* exceeded the density of *CAR* cells that expressed *IFNG* in all samples and correlated with the density of *CAR* cells that expressed *IFNG* (Kendall tau = 0.94, $P < 0.001$; Supplemental Figure 3D). Overall, the proportion of non-*CAR* cells that expressed *IFNG* was strongly correlated with the proportion of *CAR* cells within the posttreatment biopsies (Pearson r = 0.88, $P = 0.02$, Figure 4I). A comparison of mIF and ISH data further revealed that the densities of T cells that were positive for Ki67 and PD-1 and, for 4 of 6 cases, immune cells that were positive for GzmB exceeded the density of immune cells that were positive for *CAR* by 5- to 10-fold (Supplemental Figure 4). Taken together, these data identify non-CAR cells as the primary source of immune cell activation and IFN-γ production within the DLBCL TME 5 or more days after CAR T cell therapy.

IL-6 is an inflammatory cytokine implicated in the etiology of CRS and found in increased levels in blood after CAR T cell infusion (15, 20, 24). To determine whether IL-6 is produced within the DLBCL TME after axicabtagene ciloleucel, we developed and used a double ISH assay to simultaneously detect *IL6* and *CAR* transcripts in cells (Figure 5A). We observed *IL6* transcripts in 13 of 14 posttreatment biopsies and exclusively in non-*CAR* cells (Figure 5, B and C). In 12 of 13 cases, *IL6* was restricted to cells with histomorphological features consistent with lymphocytes and macrophages. We found a significantly higher percentage of *IL6*-expressing non-*CAR* immune cells in biopsies with *CAR* cells than those without *CAR* cells (median 6.0% vs. 0.3%, $P = 0.004$; Figure 5D). Unexpectedly, we also observed *IL6* widely expressed by the malignant cells in one case (Supplemental Figure 5). We conclude that the DLBCL TME is a source of IL-6 associated with local CAR T cell activation, but IL-6 is predominantly produced by non-CAR cells.

Discussion

Until recently, patients with relapsed or refractory DLBCL following treatment with combination chemotherapy and rituximab (R-CHOP) and second-line salvage therapy have had few treatment options and poor prognosis (25, 26). Axicabtagene ciloleucel has shown unprecedented efficacy in this setting, with an objective response rate of 82%, complete response rate of 54%, and a durable response rate of 42% (11, 19). As a result, axicabtagene ciloleucel is FDA-approved as third-line therapy for patients with relapsed/refractory DLBCL. Despite this success, the therapy fails to provide long-term therapeutic benefit to approximately 50% of patients. In addition, axicabtagene ciloleucel is associated with significant toxicity, including grade 3 or greater cytopenias, neurotoxicity, and/or CRS in up to 95% of patients (11). IL-6 has been implicated in the etiology of CRS but the origins of IL-6 and biological bases for additional AEs remain poorly understood (15, 27). Therefore, there has been great interest in uncovering the mechanisms underlying CAR T cell treatment efficacy, resistance, and toxicity.

This study is potentially the first extensive histopathological examination the DLBCL TME following axicabtagene ciloleucel in humans and yielded several unexpected results. First, we found a marked paucity of CAR-expressing T cells by immunohistochemical or in situ studies within the TME at all time points 5 or more days after therapy. In ZUMA-1, peripheral CAR T cells continuously increased during the first 2 weeks following product infusion, reached a maximum of 50–100 cells/microliter by day 14 (consisting of 2%–60% of all peripheral T cells), and slowly declined thereafter (11, 28). In contrast to these results, we detected no

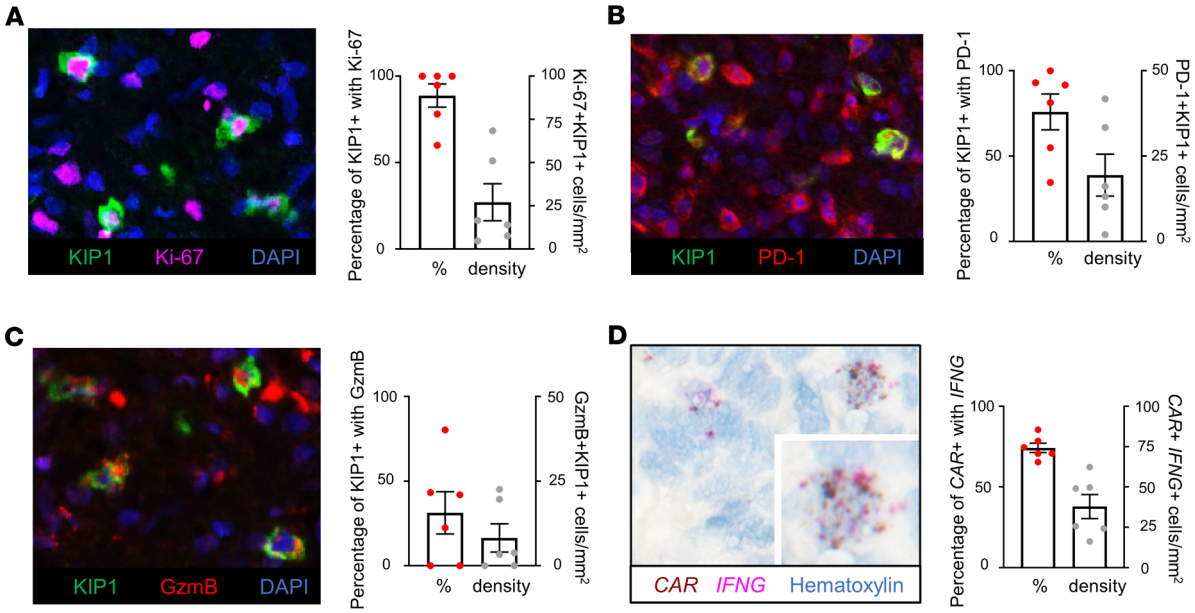

Figure 3. Expression of activation markers by CAR T cells. (**A**) A representative mIF image of a biopsy following axicabtagene ciloleucel infusion stained with anti-CAR (KIP1, green) and anti–Ki-67 (magenta) antibodies demonstrating CAR-expressing cells in cell cycle, and the percentages of Ki-67–positive CAR cells among total CAR cells and the densities of Ki-67–positive CAR cells across cases. (**B**) The case shown in **A** stained with anti-CAR (KIP1, green) and anti–PD-1 (red), showing PD-1–positive CAR cells, and the percentages of PD-1–positive CAR cells among total CAR cells and densities of PD-1–positive CAR cells across cases. (**C**) A representative image of the case shown in **A** stained with anti-CAR (KIP1, green) and anti–granzyme B (GzmB, red), and showing GzmB-positive CAR cells, and the percentages of GzmB-positive CAR cells among total CAR cells and densities of GzmB-positive CAR cells across cases. (**D**) A representative image of the case shown in **A**, hybridized with anti-*CAR* (brown) and anti-*IFNG* (red) probes showing coexpression of the *CAR* and *IFNG* transcripts in a subset of cells, and the percentages of *CAR*-positive cells with coexpression of *IFNG* among total *CAR*-positive cells and densities of *CAR*-positive cells with coexpression of *IFNG* across cases. Error bars indicate mean ± SEM. $n = 6$ in all panels. Original magnification, ×200 (**A**–**D**, including inset).

CAR-expressing T cells within DLBCL TME ≥10 days after axicabtagene ciloleucel, and when detected at earlier time points, they were in small numbers. The reasons for this discrepancy are unclear, but possibilities include inefficient migration of CAR T cells from peripheral blood into the DLBCL TME and/or rapid exit of CAR T cells from the TME following activation. In addition, we cannot rule-out the possibility that there are large numbers of intratumoral CAR T cells at earlier time points than tested in this study, (i.e., 1–3 days following infusion) and which have largely disappeared from the TME by day 5. Such a "hit-and-run" model is supported by the kinetics of activation markers on peripheral CAR T cells, which show reduced detection before day 5 (28). Examination of biopsy specimens collected at earlier time points will prove useful in evaluating this possibility and could carry significant correlative potential.

Another possibility, which we considered, is downregulation of CAR protein within the TME. Detailed kinetic studies have shown that surface CAR protein can transiently decrease when CAR T cells initially engage CD19 due to receptor internalization (29). This effect primarily occurs for CAR vectors driven by endogenous cell promoters (such as *TRAC* or *B2M*) rather than vectors driven by strong retroviral promoters, as in the case of axicabtagene ciloleucel (29). Nevertheless, we performed a highly sensitive ISH assay to address this possibility and found low numbers of cells expressing *CAR* transcript within the TME in support of the mIF findings.

Second, we found that the majority of non-CAR T cells express markers of ongoing or prior activation in biopsies taken after therapy. The origins of these non-CAR immune cells are unclear, but they may consist of nontransduced T cells included in the axicabtagene ciloleucel product or resident non-CAR immune cells within the TME before product infusion (5–7). While the preconditioning regimen consisting of cyclophosphamide and fludarabine is profoundly lymphodepleting, there are residual endogenous lymphocytes and other immune cells at the CAR T cell infusion time point (30). Regardless of origin, at least some of the factors generated by these cells, such as GzmB and IFN-γ, are known to promote both acute and long-term antitumor immunity (23). These data raise the possibility that CAR T cells may execute antitumor activity through 2 complementary mechanisms, (a) immediate killing of malignant cells via the release of cytotoxic factors following engagement of CD19 and (b) initiation of a local immune response,

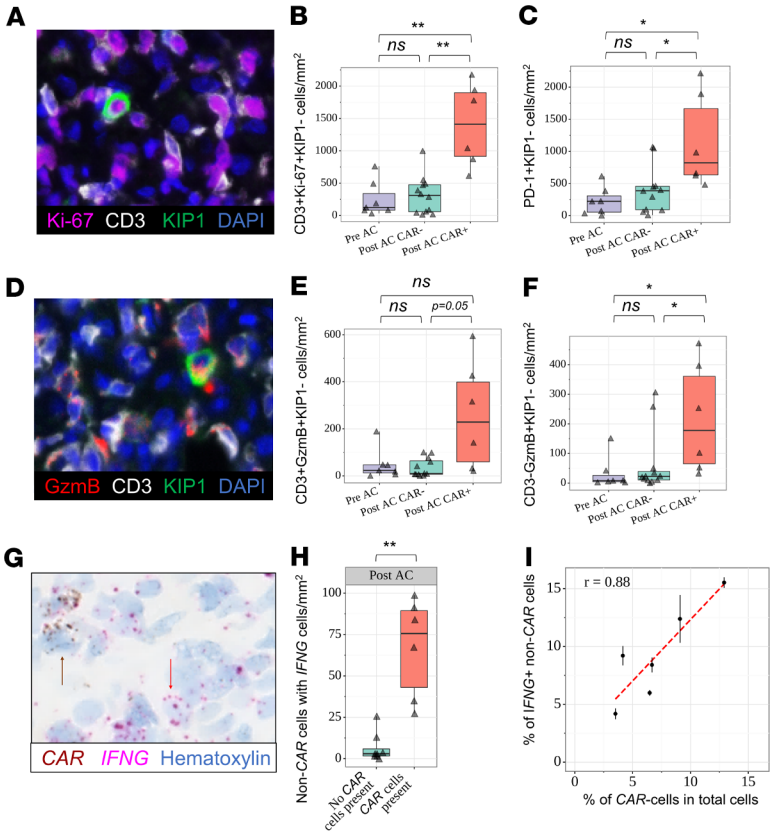

Figure 4. Non-CAR T cell activation before, and following, axicabtagene ciloleucel. Representative multiplex IF (**A** and **D**) and ISH (**G**) staining and quantitative image analysis data (**B**, **C**, **E**, **F**, **H**, and **I**) from biopsy samples obtained before axicabtagene ciloleucel infusion (*Pre AC* [*n* = 7, purple]) and following axicabtagene ciloleucel infusion (*Post AC*) further divided according to whether or not CAR T cells were detected in the corresponding biopsy sample (*CAR*$^-$ [*n* = 12, green] and *CAR*$^+$ [*n* = 6, red]). (**A**) Representative mIF staining with anti-Ki67 (magenta), anti-CD3 (white), anti-CAR (KIP1, green), and DAPI (blue) in a biopsy obtained 7 days after axicabtagene ciloleucel. (**B**) The densities of non-CAR T cells in cell cycle (*CD3*$^+$*Ki67*$^+$*CAR*$^-$) for cases in the indicated sample groups. The Kruskal-Wallis (KW) test indicated a significant difference in cell densities between conditions (*P* = 0.003). (**C**) The densities of non-CAR T cells expressing PD-1 (*CD4*$^+$*PD1*$^+$*CAR*$^-$ and *CD8*$^+$*PD1*$^+$*CAR*$^-$) for cases in the indicated sample groups. One of the twelve *CAR*$^-$ samples could not be evaluated (*n* = 11). The KW test was significant (*P* = 0.006). (**D**) Representative mIF staining with anti-GZMB (red), CD3 (white), anti-CAR (KIP1, green), and DAPI (blue) in a biopsy obtained 7 days after axicabtagene ciloleucel. (**E**) The densities of non-CAR T cells expressing granzyme B (*CD3*$^+$*GzmB*$^+$*CAR*$^-$) for cases in the indicated sample groups. The KW test was significant (*P* = 0.04). (**F**) The densities of non-CAR and non–T immune cells expressing granzyme B (*CD3*$^-$*GzmB*$^+$*CAR*$^-$) for cases in the indicated sample groups. The KW test was significant (*P* = 0.01). Brackets above the box-and-whisker plots (**B**, **C**, **E**, and **F**) indicate comparators in 2-sided Mann-Whitney *U* test followed by Benjamini-Hochberg (BH) correction for multiple tests. *adjusted *P* < 0.05, **adjusted *P* < 0.01. (**G**) Representative multiplex ISH staining with antisense probes for *CAR* transcripts (brown) and/or *IFNG* transcripts (red) in a biopsy obtained 7 days after axicabtagene ciloleucel. Arrows identify individual cells positive for *CAR* (brown arrow) and *IFNG* (red arrow). (**H**) The densities of non-*CAR* cells expressing *IFNG* transcript for cases divided according to whether *CAR*-expressing cells were or were not detected in the biopsy. Two-sided Mann-Whitney *U* test. **$P < 0.01$. (**I**) Correlation between the percentage of total cells expressing *CAR* transcripts and the percentage of non-*CAR* cells expressing *IFNG* transcripts among biopsy samples with *CAR* positive cells detected. Pearson correlation *P* = 0.02, r = 0.88. Error bars represent mean ± SEM. Original magnification, ×200 (**A** and **D**).

which amplifies and sustains the antitumor activity, leading to complete tumor resolution in a subset of patients. This is consistent with the hypothesis that a common final pathway leading to successful complete resolution of a malignant process involves a concerted immune attack against multiple targets, including the malignant cells and patient-specific epitopes resulting from somatic mutations (31).

Third, we found that non-CAR cells in the DLBCL TME were a source of IL-6 after axicabtagene ciloleucel. IL-6 is at least partially responsible for CRS in humans and in animal models, and increased serum levels of IL-6, IL-10, and IL-15 were associated with CRS and neurotoxicity of grade 3 or higher in the ZUMA-1 trial (11). IL-6 blockade with tocilizumab, a humanized IL-6 receptor, has proven an effective therapy for CRS (18, 27). By a double ISH assay, we found that IL-6 production was restricted to non-CAR

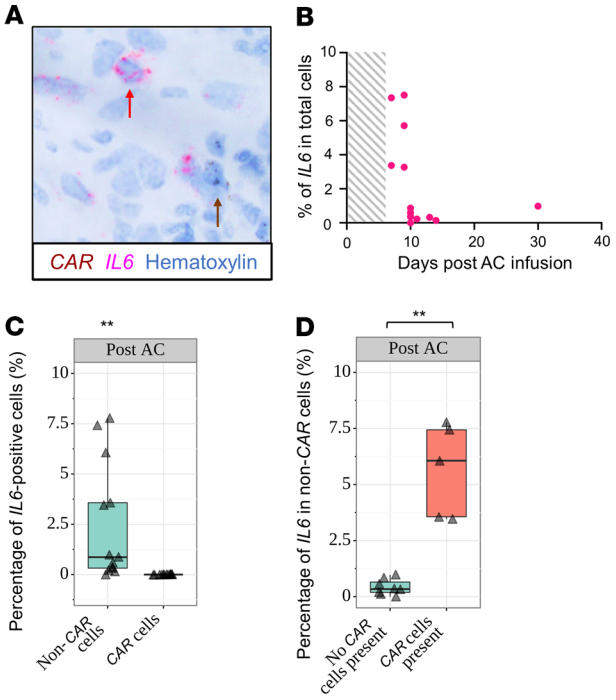

Figure 5. IL6 expression by non-CAR cells within the DLBCL microenvironment after axicabtagene ciloleucel. (**A**) Representative duplex ISH staining with anti-*CAR* (brown) and anti-*IL6* (red) probes and counterstained with hematoxylin (blue). (**B**) The number of days after axicabtagene ciloleucel infusion a biopsy was obtained and the percentage of cells expressing *IL6* transcripts (case with *IL6* expression in malignant cells excluded). Each dot represents the average number from 3 images per sample. (**C**) Percentage of *IL6*-expressing cells divided into cells that coexpress *CAR* transcript (*CAR cells*) or not (*non-CAR cells*) across all biopsies obtained after axicabtagene ciloleucel infusion (Post AC, n = 13) and showing that *IL6* production is restricted to non-*CAR* cells. One-sided, one-sample t test against an expected mean of 0. $^{**}P < 0.01$. (**D**) Percentage of non-*CAR* cells expressing *IL6* across all biopsies after axicabtagene ciloleucel infusion (n = 13) and divided into those in which *CAR* cells were detected [*CAR cells present*, n = 5] or not detected [*No CAR cells present*, n = 8] in the TME. Two-sided Mann-Whitney U test. $^{**}P < 0.01$. Original magnification, ×200 (**A**).

cells, and, in most instances, these non-CAR cells had the histomorphological features of lymphocytes and macrophages. These results are consistent with animal models of CRS in which tumor-infiltrating macrophages have been identified as a major source of IL-6 (32, 33). The non-CAR cell origin of IL-6 is also consistent with a postmortem examination of a patient with B-lymphoblastic leukemia, treated with a distinct CAR product, in which a nonmalignant cell population was identified a major source of the cytokine (34). We are currently developing assays to further define the cell lineages responsible to IL-6 within the DLBCL TME. Regardless of the source, we found the greatest numbers of IL-6–producing cells in posttreatment biopsies with CAR T cells; consistent with the notion that IL-6 production by non-CAR cells is an indirect effect of CAR T cell activation through a yet to be determined mechanism (35). Our finding of IL-6 production by non-CAR cells within the DLBCL TME does not eliminate the possibility of additional sources of IL-6 within patients, however.

Finally, we found marked IL-6 production by the malignant B cells in one case. Activated nonmalignant B cells and a subset of DLBCLs produce IL-6 which serves as an autocrine growth factor (36–38). Although a preliminary result, our finding raises the possibility that patients with specific subsets of DLBCL may be predisposed to CRS due to IL-6 production by malignant cells. An examination of larger numbers of DLBCL biopsies before and following axicabtagene ciloleucel will allow us to determine the prevalence and significance of DLBCL-associated IL-6 production in more detail.

Taken together, our data suggest a model wherein small numbers of activated CAR T cells support the activation of larger numbers of immune cells that lack CAR and contribute to the antitumor activity but also immune-mediated pathology (Figure 6). This model requires additional validation but suggests several testable hypotheses and follow-up studies. For instance, a robust, intratumoral T cell infiltrate before axicabtagene ciloleucel might indicate a TME "primed" for immune cell activation by CAR T cells.

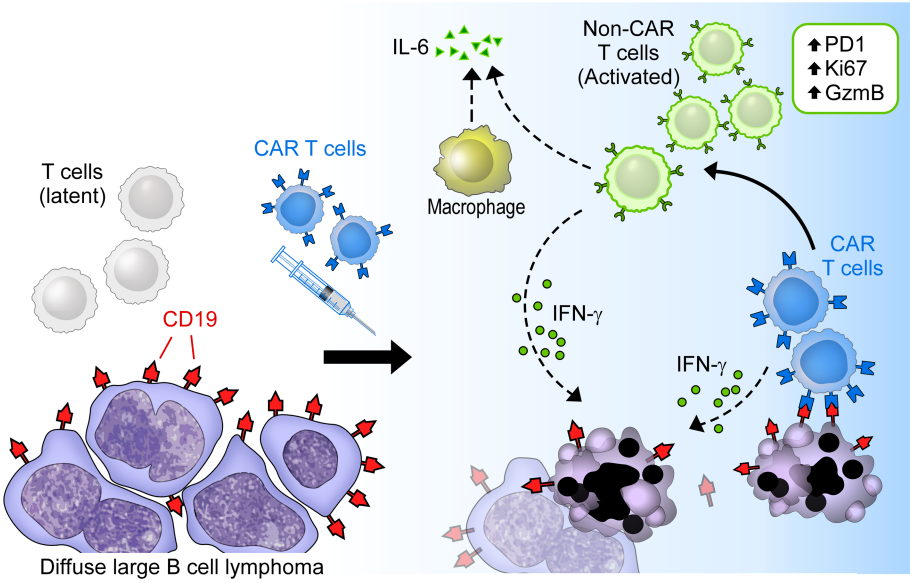

Figure 6. Model of CAR T cell–mediated antitumor immunity. CAR T cells, activated by their cognate antigen CD19, show hallmarks of activation and dysfunction, including Ki-67, granzyme B (GzmB), IFN-γ, and PD-1 expression, but constitute a minority of immune cells in the TME ≥5 days after axicabtagene ciloleucel infusion. CAR T cells stimulate non-CAR T cells and other immune cells in a manner that both supports an antitumor immune response, as exemplified by increased expression of Ki-67, GzmB, and IFN-γ and preferential expansion of $CD8^+$ $PD\text{-}1^+$ non-CAR T cells, and contributes to toxicity, as exemplified by IL-6 production by non-CAR cells.

We are currently exploring whether increased numbers of intratumoral T cells before therapy is predictive of better response or long-term outcome with axicabtagene ciloleucel. It is also possible that biomarkers predictive of response to immune checkpoint blockade, including PD-1, PD-L1, and tumor mutation burden, might also predict response to CAR T cell therapy (39–43). Such results would support trials paring CAR T cell therapy with PD-1 or PD-L1 blockade, some of which are underway (41). Future studies that use single-cell RNA sequencing will further elucidate the spectrum of cytokine and chemokine production by CAR and non-CAR T cells within the TME. It will also be important to validate candidate gene products identified in such studies using ex vivo short-term tumor cell culture systems to gain greater mechanistic insight into CAR T cell–mediated changes to the TME (44–46).

To date, the development of next-generation CAR T cell products have focused on modifications to the CAR to alter the magnitude or quality of T cell activation (42, 47–49), thus enabling a direct activity of CAR T cells on malignant cells strictly via the engagement of the cognate antigen. Our data suggest that modifications that enhance the numbers and immunoregulatory functions of CAR T cells and non-CAR T cells in the TME may also augment antitumor activity (50). For instance, engineered cell surface expression of the select cell trafficking molecules, such as CXCR4 or CCR7, might enhance CAR T cell migration to and retention in lymphoid tissues (51). Similarly, CAR T cells engineered to produce proteins that shape local immunity in a beneficial manner, such as IL-12, IL-15, and IL-18 to promote a Th1 response, or a truncated IL-6 receptor to sequester local IL-6, may augment tumoricidal activity without increasing immune-mediated pathology (23, 43).

In summary, we developed reagents to detect CAR T cells in a series of fixed biopsy specimens by mIF and ISH and demonstrate that CAR-expressing T cells express markers of activation when detected in situ but constitute a small minority of activated T cells within the DLBCL TME even at times of maximum CAR T cell expansion within peripheral blood. These data suggest role for CAR T cells in activating non-CAR immune cells, which, in turn, can further enhance tumoricidal activity but also the risk of immune-mediated AEs. This knowledge should inform the design of the next generation of engineered CAR T cells to deliver select immunostimulatory and inhibitory molecules to the TME and sculpt a more effective antitumor immune response with less toxicity. Finally, these data point to the utility of analyzing the TME very early after T cell infusion and may have a significant effect on designing next-generation autologous and "off-the-shelf" therapies.

Methods

Tissue samples. FFPE whole tissues from tumors biopsied during the ZUMA-1 trial were provided by Kite. H&E-stained tissue sections were reviewed by an expert hematopathologist, and 7 pretreatment baseline tissues and 18 posttreatment samples were selected for the study, based on the availability of high-quality, excision biopsy tissue. These samples included 4 paired samples before and after axicabtagene ciloleucel, although the paired biopsies were taken from different anatomic sites. Fifteen randomly selected diagnostic DLBCL biopsy samples were obtained from the archives of Brigham and Women's Hospital, with institutional review board approval (2010P002736), to serve as a control group. The area of the biopsy tissues analyzed by mIF were verified by a pathologist and included all tissue within the biopsy, excluding nonviable (i.e., necrotic) or normal nonlymphoid tissue (i.e., fat).

Anti-CAR antibodies and anti-CAR ISH probe. KIP1 and KIP3 antibodies were generated by Kite and recognize the Whitlow linker linear epitope joining ScFV heavy and light chains of the chimeric receptor. KIP3 was additionally confirmed as an anti-idiotype antibody binding to the broader FMC63 ScFV of axicabtagene ciloleucel. Methods for KIP1 and KIP3 immunostaining were established by chromogenic IHC and then extended to the single immunofluorescence and then mIF assays using FFPE control cells either previously transduced or not with retrovirus encoding the *CAR* transgene. Anti-*CAR* ISH probe was generated against a sequence specific to the *CAR FcV* transcript by Advanced Cell Diagnostics (Hayward, catalog 447891) based upon a published sequence (GeneBank HM852952.1). Validation was performed on FFPE cells either transduced or not with retrovirus, as described above, with similar results. Cells with one or more transcripts were scored as positive.

mIF. mIF staining was performed overnight on BOND RX fully automated stainers (Leica Biosystems) using published protocols (52–55). Briefly, 5-μm-thick FFPE tissue sections were baked for 3 hours at 60°C before loading into the BOND RX. Deparaffinization, rehydration and antigen retrieval were all preprogrammed and executed by the BOND RX. Antigen retrieval was performed in BOND Epitope Retrieval Solution 1 (ER1, Leica Biosystems) at pH 6 for 10 minutes at 98°C. Slides were serially stained with the primary antibody, secondary antibody, and the corresponding Opal fluorophore reagent as described previously (52, 54, 55) and serially repeated for all antibodies/fluorescent dyes used in the mIF panels (Supplemental Table 2). Slides were then air dried, mounted with Prolong Diamond Anti-fade mounting medium (P36965, Life Technologies) and stored in a light-proof box at 4°C before imaging.

Fluorescent image acquisition and cell phenotyping. Image acquisition was performed using the Mantra multispectral imaging platform (Akoya Biosciences) (52–54). Areas with nontumor or residual normal tissue were excluded from the analysis. Representative regions of interest were chosen by the pathologist, and 3–5 fields of view (FOVs) were acquired at ×20 resolution as multispectral images. After image capture, the FOVs were spectrally unmixed and then analyzed using supervised machine learning algorithms within Inform 2.4 (Akoya). The image analysis software assigned phenotypes to all cells in the image, based on a combination of immunofluorescence characteristics associated with segmented nuclei (DAPI signal). Each cell-phenotype specific algorithm was based upon an iterative training/test process, whereby a small number of cells are manually selected as being most representative of each phenotype of interest, and the algorithm then predicted the phenotype for all remaining cells (54, 55). Thresholds for positive staining and the accuracy of phenotypic algorithms were optimized and confirmed by the pathologist for each case.

ISH. In situ detection of RNA transcripts was performed by an automatic method using RNAscope kits (Advanced Cell Diagnostics) according to the manufacturer's instructions. Briefly, 5-μm FFPE tissue sections were pretreated by heating and protease application before hybridization with probes targeting *CAR scFv*, *IFNG*, and *IL6*. Stained slides were imaged under white light on the Mantra imaging platform (Akoya) and quantified with Inform software.

Statistics. Statistical evaluations of the data were performed with the python "scipy" package (version 1.2.0) and R (version 3.6.1). An α of 0.05 was used as a threshold for significance. The abbreviation "ns" indicates a nonsignificant relationship, where evidence failed to meet that α threshold. Sample-derived quantities were compared across categories by a 2-tailed Mann-Whitney *U* test unless otherwise specified. When more than 2 conditions were compared within an experiment a Kruskal-Wallis (KW) 1-way analysis of variance was used to test the hypothesis that the samples originated from the same distribution; the KW test results are included in all relevant figure legends. Furthermore, individual *P* values within experiments with more than 2 comparisons were adjusted for multiple tests (all pairwise combinations of conditions)

using the Benjamini-Hochberg procedure; these are reported in the text and legends as adjusted *P* values. Since CAR cells did not express IL-6, a 1-sided 1-sample (1-tailed) *t* test was used to test if non-CAR IL-6 expression was greater than 0. Correlations of activation markers were measured by a Kendall rank correlation (tau), other correlations were measured as a Pearson correlation (r). For the box-and-whisker plots, the triangles represent the individual sample values, the horizontal center lines represent medians, boxes demarcate 25th to 75th percentiles, and vertical lines (whiskers) represent the range.

Study approval. Fifteen randomly selected diagnostic DLBCL biopsy samples were obtained from the archives of Brigham and Women's Hospital, with institutional review board approval (2010P002736), to serve as a control group. Informed consent was waived by the institutional review board.

Author contributions

PHC, CJ, PA, KW, FSH, SJR, ZJR, JR, AB, and WG designed and planned studies. PHC and ML carried out the experiments. PHC, ML, JLW, JR, and AB contributed to data acquiring and analysis. SAS, ZJR, JR, AB, and WG provided reagents. PHC and SJR wrote the manuscript with input from all authors. The co–first authorship order was assigned by last name alphabet.

Acknowledgments

This work was supported by Kite, a Gilead company. We thank Anita Giobbie-Hurder (Biostatistician, Division of Biostatistics, Department of Data Sciences, Dana-Farber Cancer Institute) for helpful advice on the statistical analysis.

Address correspondence to: Scott J. Rodig, Department of Pathology, Brigham and Women's Hospital, Boston, Massachusetts 02115, USA. Phone: 617.525.7825; Email: srodig@bwh.harvard.edu.

1. Brudno JN, Kochenderfer JN. Chimeric antigen receptor T-cell therapies for lymphoma. *Nat Rev Clin Oncol*. 2018;15(1):31–46.
2. Boyiadzis MM, et al. Chimeric antigen receptor (CAR) T therapies for the treatment of hematologic malignancies: clinical perspective and significance. *J Immunother Cancer*. 2018;6(1):137.
3. June CH, Sadelain M. Chimeric antigen receptor therapy. *N Engl J Med*. 2018;379(1):64–73.
4. Locke FL, et al. Phase 1 results of ZUMA-1: a multicenter study of KTE-C19 anti-CD19 CAR T cell therapy in refractory aggressive lymphoma. *Mol Ther*. 2017;25(1):285–295.
5. Schuster SJ, et al. Chimeric antigen receptor T cells in refractory B-cell lymphomas. *N Engl J Med*. 2017;377(26):2545–2554.
6. Gill S, June CH. Going viral: chimeric antigen receptor T-cell therapy for hematological malignancies. *Immunol Rev*. 2015;263(1):68–89.
7. Grupp SA, et al. Chimeric antigen receptor-modified T cells for acute lymphoid leukemia. *N Engl J Med*. 2013;368(16):1509–1518.
8. Maude SL, et al. Chimeric antigen receptor T cells for sustained remissions in leukemia. *N Engl J Med*. 2014;371(16):1507–1517.
9. Levin A, Shah NN. Chimeric antigen receptor modified T cell therapy in B cell non-Hodgkin lymphomas. *Am J Hematol*. 2019;94(S1):S18–S23.
10. Roberts ZJ, Better M, Bot A, Roberts MR, Ribas A. Axicabtagene ciloleucel, a first-in-class CAR T cell therapy for aggressive NHL. *Leuk Lymphoma*. 2018;59(8):1785–1796.
11. Neelapu SS, et al. Axicabtagene ciloleucel CAR T-cell therapy in refractory large B-cell lymphoma. *N Engl J Med*. 2017;377(26):2531–2544.
12. Schuster SJ. CD19-directed CAR T cells gain traction. *Lancet Oncol*. 2019;20(1):2–3.
13. [No authors listed]. YESCARTA Prescribing Information. YESCARTA. https://www.yescarta.com/files/yescarta-pi.pdf. Accessed May 27, 2020.
14. Nair R, Neelapu SS. The promise of CAR T-cell therapy in aggressive B-cell lymphoma. *Best Pract Res Clin Haematol*. 2018;31(3):293–298.
15. Galon J, et al. Characterization of anti-CD19 chimeric antigen receptor (CAR) T cell-mediated tumor microenvironment immune gene profile in a multicenter trial (ZUMA-1) with axicabtagene ciloleucel (axi-cel, KTE-C19). *J Clin Oncol*. 2017;35(15_suppl):3025.
16. Rossi JM, et al. Clinical response in ZUMA-1, the pivotal study of axicabtagene ciloleucel (Axi-Cel) in patients with refractory large B cell lymphoma, may be influenced by characteristics of the pretreatment tumor microenvironment (TME). *Clin Lymphoma Myeloma Leuk*. 2018;18:S281.
17. Rossi JM, et al. Abstract CT153: Pretreatment immunoscore and an inflamed tumor microenvironment (TME) are associated with efficacy in patients (Pts) with refractory large B cell lymphoma treated with axicabtagene ciloleucel (Axi-Cel) in ZUMA-1. *Cancer Res*. 2019;79(13 Supplement):CT153.
18. Brudno JN, Kochenderfer JN. Recent advances in CAR T-cell toxicity: Mechanisms, manifestations and management. *Blood Rev*. 2019;34:45–55.
19. Locke FL, et al. Long-term safety and activity of axicabtagene ciloleucel in refractory large B-cell lymphoma (ZUMA-1): a single-arm, multicentre, phase 1-2 trial. *Lancet Oncol*. 2019;20(1):31–42.
20. Locke FL, et al. Abstract CT020: Immune signatures of cytokine release syndrome and neurologic events in a multicenter reg-

istrational trial (ZUMA-1) in subjects with refractory diffuse large B cell lymphoma treated with axicabtagene ciloleucel (KTE-C19). *Cancer Res*. 2017;77(13 Supplement):CT020.
21. Khan O, et al. TOX transcriptionally and epigenetically programs CD8+ T cell exhaustion. *Nature*. 2019;571(7764):211–218.
22. Scott AC, et al. TOX is a critical regulator of tumour-specific T cell differentiation. *Nature*. 2019;571(7764):270–274.
23. Dunn GP, Koebel CM, Schreiber RD. Interferons, immunity and cancer immunoediting. *Nat Rev Immunol*. 2006;6(11):836–848.
24. Hirayama AV, Turtle CJ. Toxicities of CD19 CAR-T cell immunotherapy. *Am J Hematol*. 2019;94(S1):S42–S49.
25. Habermann TM. New developments in the management of diffuse large B-cell lymphoma. *Hematology*. 2012;17 Suppl 1:S93–S97.
26. Crombie JL, Armand P. Diffuse large B-cell lymphoma and high-grade B-cell lymphoma: genetic classification and its implications for prognosis and treatment. *Hematol Oncol Clin North Am*. 2019;33(4):575–585.
27. Le RQ, et al. FDA approval summary: tocilizumab for treatment of chimeric antigen receptor T cell-induced severe or life-threatening cytokine release syndrome. *Oncologist*. 2018;23(8):943–947.
28. Kochenderfer JN, et al. B-cell depletion and remissions of malignancy along with cytokine-associated toxicity in a clinical trial of anti-CD19 chimeric-antigen-receptor-transduced T cells. *Blood*. 2012;119(12):2709–2720.
29. Eyquem J, et al. Targeting a CAR to the TRAC locus with CRISPR/Cas9 enhances tumour rejection. *Nature*. 2017;543(7643):113–117.
30. Kochenderfer JN, et al. Chemotherapy-refractory diffuse large B-cell lymphoma and indolent B-cell malignancies can be effectively treated with autologous T cells expressing an anti-CD19 chimeric antigen receptor. *J Clin Oncol*. 2015;33(6):540–549.
31. Tran E, Robbins PF, Rosenberg SA. 'Final common pathway' of human cancer immunotherapy: targeting random somatic mutations. *Nat Immunol*. 2017;18(3):255–262.
32. Giavridis T, van der Stegen SJC, Eyquem J, Hamieh M, Piersigilli A, Sadelain M. CAR T cell-induced cytokine release syndrome is mediated by macrophages and abated by IL-1 blockade. *Nat Med*. 2018;24(6):731–738.
33. Norelli M, et al. Monocyte-derived IL-1 and IL-6 are differentially required for cytokine-release syndrome and neurotoxicity due to CAR T cells. *Nat Med*. 2018;24(6):739–748.
34. Obstfeld AE, et al. Cytokine release syndrome associated with chimeric-antigen receptor T-cell therapy: clinicopathological insights. Blood. 2017;130(23):2569–2572.
35. Garfall AL, et al. T-cell phenotypes associated with effective CAR T-cell therapy in postinduction vs relapsed multiple myeloma. *Blood Adv*. 2019;3(19):2812–2815.
36. Arkatkar T, et al. B cell-derived IL-6 initiates spontaneous germinal center formation during systemic autoimmunity. *J Exp Med*. 2017;214(11):3207–3217.
37. Lu L, et al. Gene regulation and suppression of type I interferon signaling by STAT3 in diffuse large B cell lymphoma. *Proc Natl Acad Sci USA*. 2018;115(3):E498–E505.
38. Hashwah H, et al. The IL-6 signaling complex is a critical driver, negative prognostic factor, and therapeutic target in diffuse large B-cell lymphoma. *EMBO Mol Med*. 2019;11(10):e10576.
39. Merryman RW, Armand P, Wright KT, Rodig SJ. Checkpoint blockade in Hodgkin and non-Hodgkin lymphoma. *Blood Adv*. 2017;1(26):2643–2654.
40. Wei SC, Duffy CR, Allison JP. Fundamental mechanisms of immune checkpoint blockade therapy. *Cancer Discov*. 2018;8(9):1069–1086.
41. Chong EA, et al. PD-1 blockade modulates chimeric antigen receptor (CAR)-modified T cells: refueling the CAR. *Blood*. 2017;129(8):1039–1041.
42. Ramos CA, et al. Clinical and immunological responses after CD30-specific chimeric antigen receptor-redirected lymphocytes. *J Clin Invest*. 2017;127(9):3462–3471.
43. Finney OC, et al. CD19 CAR T cell product and disease attributes predict leukemia remission durability. *J Clin Invest*. 2019;129(5):2123–2132.
44. Jenkins RW, et al. *Ex vivo* profiling of pd-1 blockade using organotypic tumor spheroids. *Cancer Discov*. 2018;8(2):196–215.
45. Guo X, et al. Global characterization of T cells in non-small-cell lung cancer by single-cell sequencing. *Nat Med*. 2018;24(7):978–985.
46. Sterner RM, et al. GM-CSF inhibition reduces cytokine release syndrome and neuroinflammation but enhances CAR-T cell function in xenografts. *Blood*. 2019;133(7):697–709.
47. Lim WA, June CH. The principles of engineering immune cells to treat cancer. *Cell*. 2017;168(4):724–740.
48. Cohen AD, et al. B cell maturation antigen-specific CAR T cells are clinically active in multiple myeloma. *J Clin Invest*. 2019;129(6):2210–2221.
49. Ruella M, et al. The addition of the BTK inhibitor ibrutinib to anti-CD19 chimeric antigen receptor T cells (CART19) improves responses against mantle cell lymphoma. *Clin Cancer Res*. 2016;22(11):2684–2696.
50. Turtle CJ, et al. Immunotherapy of non-Hodgkin's lymphoma with a defined ratio of CD8+ and CD4+ CD19-specific chimeric antigen receptor-modified T cells. *Sci Transl Med*. 2016;8(355):355ra116.
51. Mishan MA, Ahmadiankia N, Bahrami AR. CXCR4 and CCR7: Two eligible targets in targeted cancer therapy. *Cell Biol Int*. 2016;40(9):955–967.
52. Stack EC, Wang C, Roman KA, Hoyt CC. Multiplexed immunohistochemistry, imaging, and quantitation: a review, with an assessment of Tyramide signal amplification, multispectral imaging and multiplex analysis. *Methods*. 2014;70(1):46–58.
53. Patel SS, et al. The microenvironmental niche in classic Hodgkin lymphoma is enriched for CTLA-4-positive T cells that are PD-1-negative. *Blood*. 2019;134(23):2059–2069.
54. Carey CD, et al. Topological analysis reveals a PD-L1-associated microenvironmental niche for Reed-Sternberg cells in Hodgkin lymphoma. *Blood*. 2017;130(22):2420–2430.
55. Keskin DB, et al. Neoantigen vaccine generates intratumoral T cell responses in phase Ib glioblastoma trial. *Nature*. 2019;565(7738):234–239.